Journal of Inorganic and Organometallic Polymers and Materials (2023) 33:254–265
https://doi.org/10.1007/s10904-022-02472-0

Hybrid Nanoarchitectonics with Cr, Fe-MOF/ Graphene Nanocomposite for Removal of Organic Sulfur Compounds from Diesel Fuel

Aya M. Matloob[1] · Dalia R. Abd El-Hafiz[1] · L. Saad[1] · S. Mikhail[1]

Received: 1 June 2022 / Accepted: 14 August 2022 / Published online: 3 October 2022

Abstract
Metal–organic frameworks (Cr-MOF and Fe-MOF) and their graphene hybride nano-composites were prepared via green solvo-themal method. The prepared samples were characterized by XRD, FTIR spectroscopy, N_2 adsorption–desorption isotherm and XPS. The composites were used for the adsorption of thiophenic sulfur compound (thiophene, dibenzothiophene, 4,6-dimethyldibenzothiophene) in a model fuel oil. It was found that, graphene in the MOF composite has positive effect on sulfur removal. The removal efficiency increase from 62% to % 95.6 using Fe-MOF and Fe-MOF/Gr (9:1), respectively. This enhancement effect is attributed to a greater number of coordinatively unsaturated sites (CUS) in the composites. The results indicated that the adsorption reach to 96.6% for DBT adsorption from model diesel oil and 62% for diesel fuel on using Cr-MOF/Gr composite.

Keywords Metal organic framework · Graphene · Green fuel · Nano composites · Sulfur compounds

1 Introduction

Deep desulfurization of liquid hydrocarbon fuels has become an increasingly important subject worldwide. The sulfur content in the transportation fuels is a very serious environmental concern. Thus, a number of countries have initiated and applied a set of strict environmental regulations and laws to reduce the sulfur contents in diesel oil to ultra-low levels (given as 10–15 ppm). The main goal of applying such strict regulations is to minimize the harmful exhaust emissions, improve air quality and limit air pollution.

Elimination of sulfur compound in transportation fuel can be achieved either by utilizing different desulfurization processes for the fuel products, which is commonly carried out using the catalytic hydrogen processing approaches, or by removing sulfur compounds contained in stack gases. Reducing the sulfur content in diesel fuel to less than 15 ppm is a complicated process [1].

HDS is the conventional process used for the removal of sulfur compounds contained in diesel oil, this process has considered a real challenge. This is due to the fact that some sulfur species contained in diesel oil have low reactivity and complicated removal mechanisms. Researchers and experts are currently enhancing these processes by synthesis of new HDS catalysts, improved reactors and optimized operating conditions were tested for the removal of certain sulfur compounds that are characterized by low reactivity [1].

Deep hydrodesulfurization process may result in changing the properties of the diesel oil, such as reducing the lubricity. This may occur due to the elimination of some compounds that are responsible for lubricity of the diesel fuel. In addition, HDS may result in reducing the density of the produced diesel oil which is directly related to a reduction in the energy content by around 1%. Moreover, producing diesel oil with ultra-low sulfur content (ULSD) (15 ppm) has higher costs compared to producing low-sulfur content diesel oil (500 ppm). However, a significant reduction in the cost of producing diesel oil with sulfur content that is less than 15 ppm can be achieved by integrating the HDS units with a non-hydrogenation process, such as adsorptive desulfurization units [1].Various adsorbents, such as reduced metals, metal oxides, activated charcoal, alumina, metal sulfides, zeolites and silica, are utilized in this process.

Metal organic frameworks (MOFs), as a class of materials constructed by metal ions and organic ligands, have been widely studied in fields of fuel storage, capture of gas, and catalyst application [2]. MOFs are promising materials for

✉ Aya M. Matloob
aya_mtloob@epri.sci.eg

[1] Refining department, Catalysis Lab, Egyptian Petroleum Research Institute, Cairo 11727, Egypt

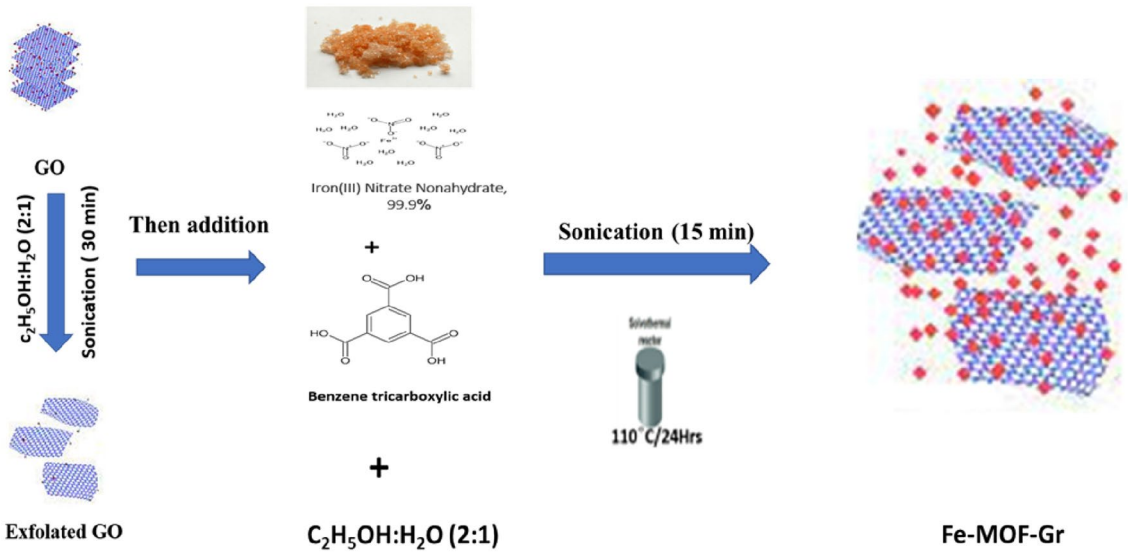

Scheme 1 Initial Figure for Solvothermal Synthesis of Fe-MOF-Gr

liquid phase adsorption applications, because of the ultra-high specific surface area and the easy tunability of their pore size and shape [3]. MOFs based novel adsorbents have shown the very promising results in removal of aromatic sulfur compounds from liquid fuel in recent years [4]. Graphene oxide (GO), two-dimensional (2D) carbon-based nanomaterial with oxygen-containing functional groups, has received tremendous interest in recent years. The interlayer distance of GO is usually between 6 and 12 ˚A [5]. Owing to its unique structure, GO has been used to build various composites materials with MOFs. MOF- GO, having covalent nature of interactions between the MOFs and GO applying the prepared hybrid nanocomposites as adsorbent.

In this paper, Fe-MOF and Cr-MOF and its graphene composites were prepared using simple, facile and green solvothermal method, then characterized using XRD, FTIR, N2 adsorption/desorption isotherms analysis. The performances of the adsorptive property of the prepared materials are investigated for the first time towards the adsorption of thiophenic compounds from the model diesel oils. Liquid phase batch adsorption experiments are performed at room temperature and under atmospheric pressure.

2 Experimental

2.1 Material Preparation

2.1.1 Preparation of (MOFs)

The MOFs, used in this study were prepared by mixed Fe(NO3)2·3H2O (1.73 g, 0.004 mmol in water) with benzene-1,3,5-tricarboxylic acid (H3BTC, 0.5 g, 0.0024 mmol, in ethanol) in tightly sealed Teflon reactor. The reactor was heated in an oven at 110 °C for 24 h, then cooled to room temperature. Brown solid products of MOF were collected and washed several times with ethanol, then dried at 70 °C for 12 h. For synthesis of Cr-MOF the metal source is Cr(NO3)3·9H2O under the same steps of the previous one.

2.1.2 Synthesis of M-BTC/ Graphene (MOF/Gr) Nanocomposites

The MOF/Gr nanocomposites used in this study were prepared as follow: (1) 1 mg/ml graphite oxide was suspended in an ethanol:water mixture (2:1 (v: v)) and sonicated for 30 min (Soln. A). (2) 1.0 g of $Fe(NO_3)_2{\cdot}3H_2O$ (0.004 mmol) and 0.5 g benzene-1,3,5-tricarboxylic acid (H_3BTC, 0.0024 mmol) were separately dissolved in 10 ml ethanol: water mixture (2:1 (v: v)) (Soln. B & C respectively). (3) The two solution A & B are mixed and vigorously sonicated for 15 min. (4) Solution C was added to the above mixture and sonicated for another 15 min. (5) The final mixture was placed into Teflon reactor and tightly sealed, and heated at 110 °C for 24 h, and then cooled to room temperature. Black solids hybrid nanocomposites were collected and washed several times with ethanol. Finally, the resulting solid was dried at 70 °C for 12 h and a fine dark black powder of MOF/Gr was obtained as shown in Scheme 1. For synthesis of Cr-MOF/Gr nanocomposite the metal source is $Cr(NO_3)_3{\cdot}9H_2O$ under the same steps of the previous one.

2.2 Material Characterization

2.2.1 X-ray Powder Diffraction Analysis (XRD)

X-ray Powder Diffraction Analysis (XRD) was used to ensure the various changes in the crystalline structure and the different phases accompanied the preparation process. Analysis was carried out using a Shimadzu XD-1 diffractometer using Cu K_α radiation ($\lambda = 0.1542$ nm) at a beam voltage of 40 kV and 40 mA beam current. The intensity data was collected at 25 °C in a 2θ range of 4–80° with a scan rate of $0.7^{\circ}s^{-1}$.

2.2.2 Fourier Transformer Infrared Spectroscopy (FTIR)

Fourier transformer infrared spectroscopy (FTIR) was used to investigate the function groups of the prepared samples. Analysis was carried out using ATI Mattson 1001 in the wave number region of 400–4000 cm^{-1}.

2.2.3 The Textural Properties

The textural properties were determined from the N_2 adsorption/desorption isotherms measured at liquid nitrogen temperature (– 196 °C) using a NOVA 3200 Unit, USA apparatus.

2.3 Adsorption Experiment

The liquid phase adsorption properties were assessed through batch adsorption experiments to compare the performance of MOF with MOF/Gr hybride nanocomposites towards the desulfurization of the model diesel fuel. A stock solution of di-benzothiophene (DBT) as a model diesel oil was prepared (1000 ppm, in dodecane). For all experiments, an exact amount of the prepared adsorbents (0.05–0.2 g) was put in 10 mL of DBT stock solutions. The mixture was then shaked using a flask shaker oscillating at 400 oscillations/min for a fixed period of time (0.5–5 h) at an ambient temperature. The adsorption equilibrium isotherms measured in a DBT concentration ranged between 200 and 1000 ppm at 25 °C for 5 h. For analysis, the solution was separated from the adsorbents by filtration and the DBT concentration was measured using GC-FPD. The adsorption capacity and desulfurization rate were calculated by the following:

$$q_i = \frac{m}{M} \times \left(C_0 - \mathrm{C}_i\right) \times 10^{-3} \quad (1)$$

$$W = \left(C_0 - \mathrm{C}_i / C_0\right) \times 100\% \quad (2)$$

where q_i is the adsorption capacity of sulfur adsorbed on the adsorbent (mg S g^{-1}), m is the mass of model oil (g), M is the mass of the MOF (g), C_0 and C_i are the initial and final S concentrations in the model oil, respectively, C_e is the equilibrium S-concentrations in the model oil.

3 Result and Discussion

3.1 Characterizations of the Prepared Samples

3.1.1 X-ray Diffraction Analysis (XRD)

X-ray diffraction analysis (XRD)of the prepared Fe-MOF samples (Fig. 1) with different Fe: BTC molar ratio (1:1, 2:1, and 3:1) emphasized that, all MOF samples displayed the same peaks (2θ° on 10.05°, 19.01°, and 24.4°) as the simulated XRD pattern which was calculated using single crystal data and published by [1], which confirming the successful synthesis of Fe-MOF. Moreover, for the samples with molar ratio 3:1 (Fe: BTC) there is another characteristic peak to Fe_2O_3 (JCPDS NO.84-0311) which is a side product due to the high Fe concentration. While, the low Fe concentration (1:1) avoids the Fe^{3+} ions reduction, and the intensity of the main diffraction peaks of Fe-MOF is lower than that of the prepared sample with molar ratio (2:1). Thus, the sample with molar ratio (2:1) is selected to complete the preparation of the Fe-MOF/Gr hybrid nano-composite sample.

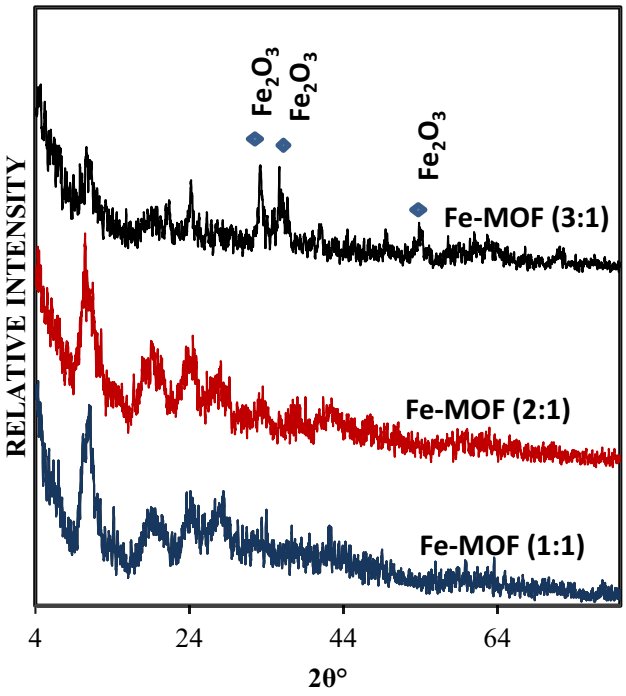

Fig. 1 XRD patterns of the prepared Fe-MOF samples

3.1.2 The XRD Pattern of the Fe-MOF/Gr (9:1) Sample

The XRD pattern of the Fe-MOF/Gr (9:1) sample is mainly consistent with that Fe-MOF (Fig. 2). No discernible diffraction peaks belonging to GO (normally at about 9.3°) be detected in the pattern of Fe-MOF/Gr. This result established that the incorporation of GO does not disturb the formation of Fe-MOF and the composites preserve the structure of Fe-MOF. Also, the absence of the characteristic peaks of GO could be ascribed to the low GO content (~ 10 wt%) and/or the exfoliation and reduction of GO in ethanol via the sonication during the synthesis procedure.

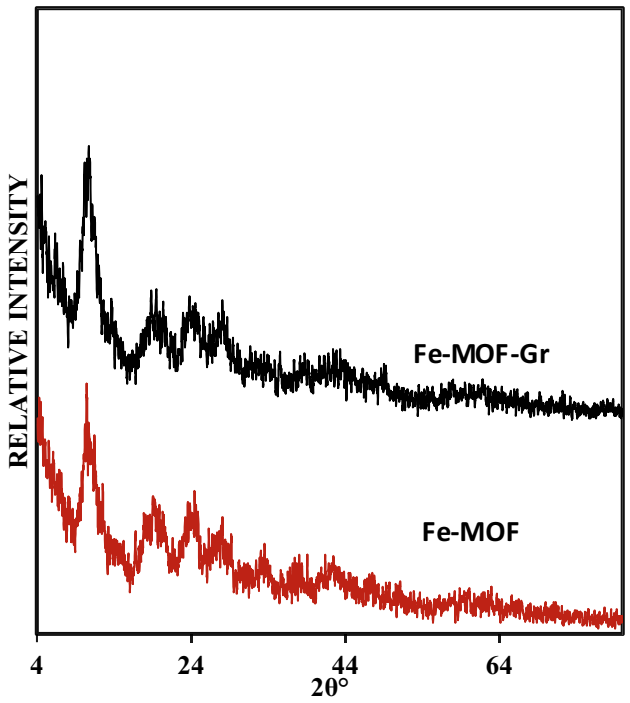

Fig. 2 XRD patterns of Fe-MOF& Fe-MOF/Graphene samples

3.1.3 FTIR Spectra of the Prepared Fe-MOF Samples

FTIR spectra of the prepared Fe-MOF samples with the different Fe: BTC molar ratio (Fig. 3) show different characteristic bands, confirming the successful synthesis of MOF structure [6]: (1) bands at 1610 cm^{-1}, and 1360 cm^{-1} are corresponding to C = O and C-O group of carboxylic acid after coordination of H_3BTC to the metal center, (2) The broad band at 3400 cm^{-1} assigned –OH groups, indicates the presence of water molecules, Furthermore, stretching vibration of –OH indicates the presence of hydrogen bonding after coordinated with iron, (3) bands at 590 and 630 cm^{-1} can be assigned to the Fe–O bonds of Fe-MOF compound, (4) bands around 1700, and 1450 cm^{-1} Correspond to the (C = O) and (C–O) stretching frequency respectively for free carboxylic groups of H_3BTC [7].

On the other hand, the decreasing the Fe: BTC molar ratio, from 2 to 1, lead to disappear of all the vibrational bands. Also, the increase of Fe: BTC molar ratio from 2 to 3 lead to a decrease of all the vibrational bands which attributed to the inhibition of MOF structure formation, in agreement with XRD data.

3.1.4 FT-IR Spectra of the Fe-MOF/Gr Hybrid Nano-Composite

FT-IR spectra of the Fe-MOF/Gr hybrid nano-composite sample with a MOF: Gr weight ratio (9:1) (Fig. 4) is similar to the spectrum of the parent Fe- MOF. On the other hand, the increase in the intensity of the peak at 729 cm^{-1} attributed to the Fe–O group formed in GO-Fe(III) [8], and the increase in the intensity of the peak at 1700 cm^{-1} be attributed to the partial replacement of the carboxylic

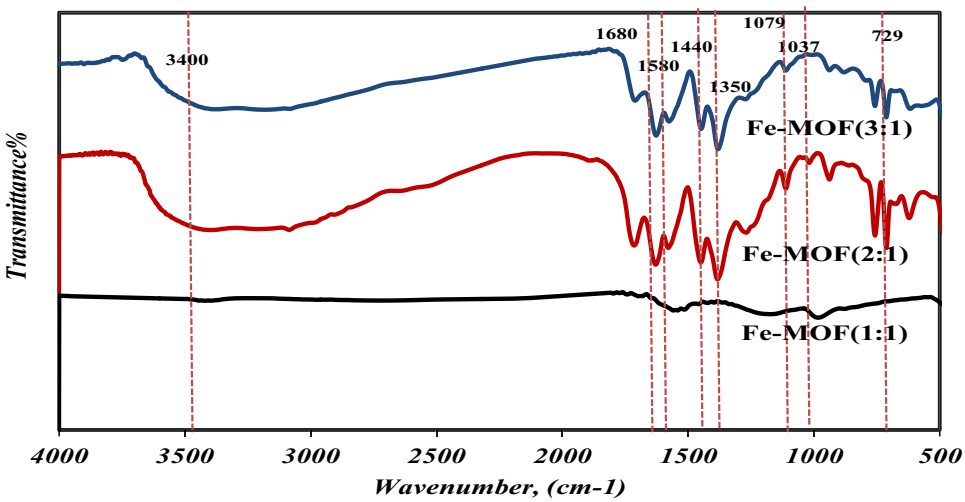

Fig. 3 FTIR spectra of the prepared Fe-MOF samples

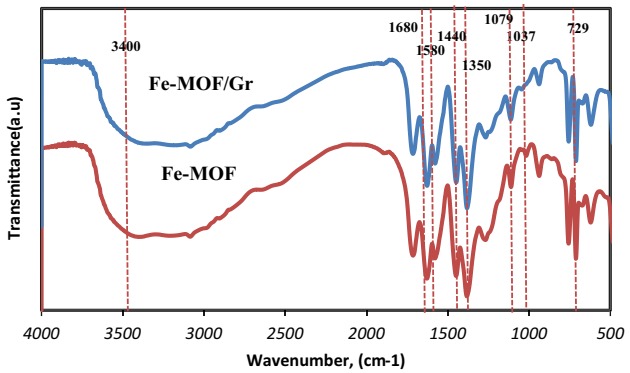

Fig. 4 FTIR spectra of Fe-MOF& Fe-MOF/Graphene samples

groups of BTC in the MOF structure. This creates a coordinate between the oxygen groups in GO and the metal center in the MOF structure, which established that the MOF and GO are well composited to form the MOF/Gr hybrid nanocomposite material.

3.1.5 Texture Properties

Texture properties of the prepared materials were investigated, using N_2 adsorption/desorption isotherms. Both Fe-MOF and Fe-MOF /Gr samples showed type-I isotherm according to Brunauer's classification which is typical for microporous materials with a high nitrogen adsorption amount (Fig. 5a).The steep at the initial region is due to strong adsorption and micro-pore filling, as indicated by v-t plot and PSD (1.5–4 nm), (Fig. 5b, c). The overlaps of adsorption and desorption curves indicated that the adsorption–desorption reaction is fully reversible.

The BET surface area, micropore surface area, pore volume, micropore volume and pore radius obtained from N_2 adsorption isotherms at low P/Po ranges are included in Table 1.

From data, the incorporation of GO in the prepared Fe-MOF sample lead to a decrease in the surface area in parallel with the increase in total pore volume (Table1). Moreover, BJH calculation shows unimodal pore size distribution with an obvious porous distribution around 2 nm (Fig. 5b). Accordingly, the slightly decrease in surface area and increase of pore structure may be attributed

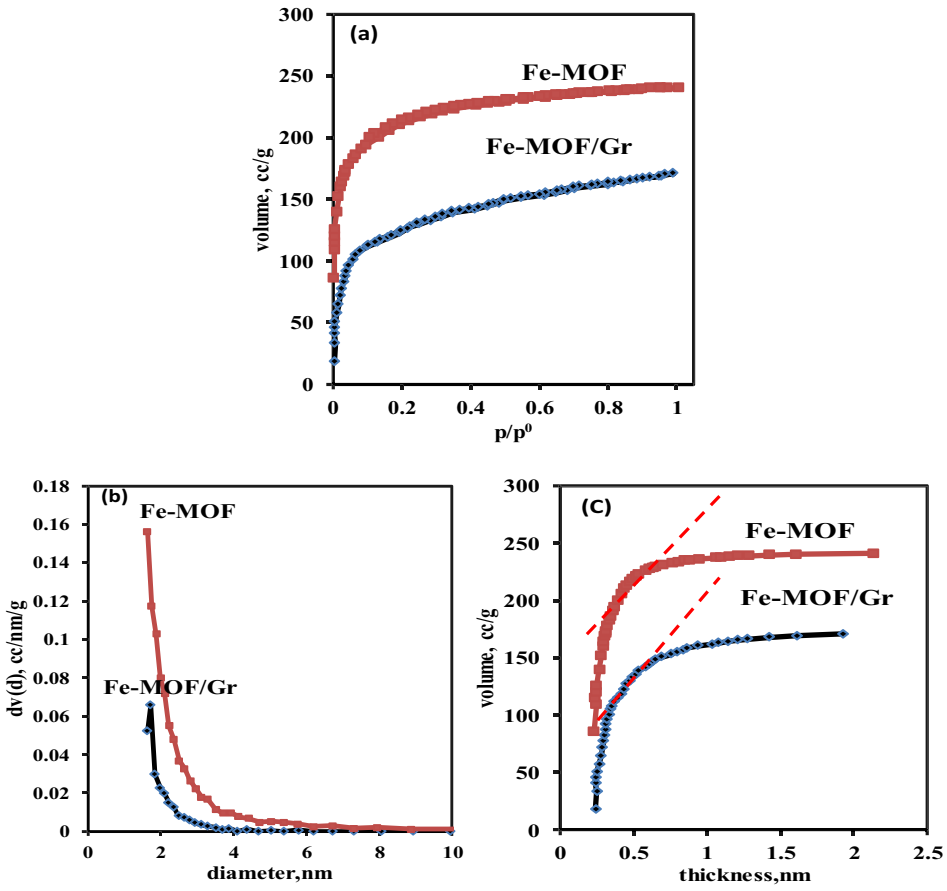

Fig. 5 **A** N_2 adsorption desorption isotherm, **B** PSD and **C** v-t plot

Table 1 BET surface characterization of the prepared Fe-MOF and Fe-MOF/Gr samples

	Surface area m^2/g	Total pore volume, cc/g	Micropore volume, cc/g	Micropore area, m^2/g	Average pore diameter, nm
Fe-MOF	640.10	0.13	0.24	539.10	2.09
Fe-MOF/Gr	400.40	0.26	0.10	272.50	2.64

to the incorporated GO (low concentration) into MOF in agreement wih Yujie Li data [9].

In the X-ray photoelectron spectroscopy spectrum of Fe 2p for Fe-MOF (Fig. 30), there are two main peaks at 711.5 and 727 eV and a satellite peak at 718.5 eV, which matches well with the Fe-MOF [10]. All the spectrum of Fe 2p for Fe-MOF/Gr show four peaks at 714, 719.2,725.6, and 728 eV, indicating that the chemical environment of Fe(III) had not changed and still bonded with benzene rings in as- prepared Fe-MOF (Fig. 6).

According to Fig. 7, the main diffraction lines of the prepared Cr-MOF samples with different Cr: BTC molar ratio (1:1, 2:1, and 3:1) are in agreement with the simulated XRD pattern which was calculated using single crystal data of MIL-100 (Cr) with the main 2θ° (10.37°, 15.12°, and 25.27°) [11], which confirming the successful synthesis of Cr-MOF.

Moreover, for the sample with molar ratio 1:1 (Cr: BTC) the intensity of the main diffraction peaks of Cr-MOF is lower than the sample of (2:1) molar ratio, while the sample with molar ratio 3:1 (Cr: BTC) there is a quite disappear for

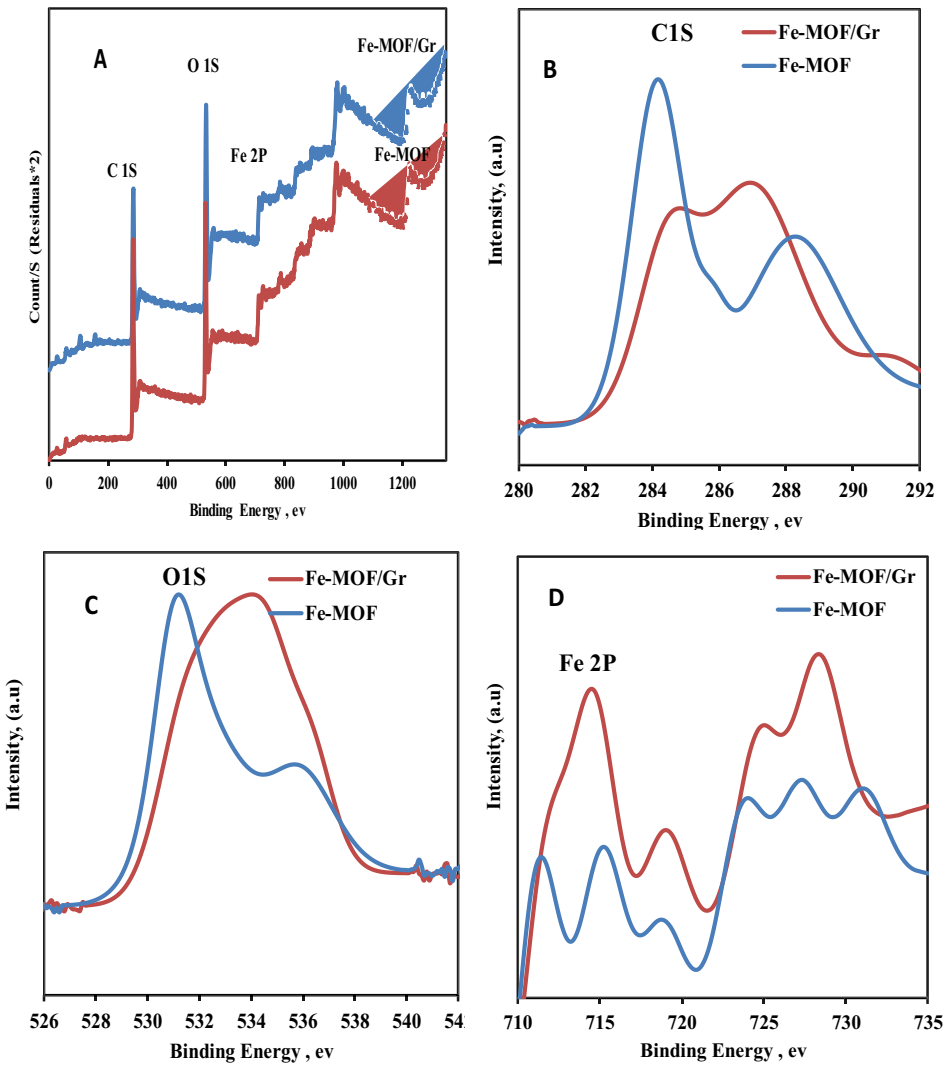

Fig. 6 **A** XPS survey analysis of Fe-MOF and Fe-MOF/Gr, **B** C1S spectra of Fe-MOF and Fe-MOF/Gr, **C** O 1 s spectra of Fe-MOF and Fe-MOF/Gr, **D** Fe 2p spectra of Fe-MOF and Fe-MOF/Gr

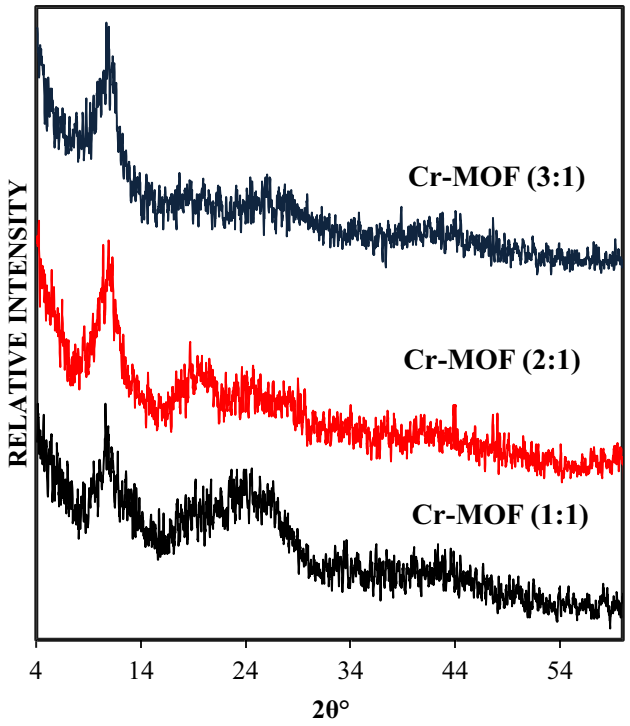

Fig. 7 XRD patterns of the prepared Cr-MOF samples

the peaks which characteristic Cr-MOF, So, this sample with (2:1) molar ratio was selected to complete the preparing of Cr-MOF/Gr hybrid nano-composite material.

3.1.6 The XRD Pattern of the Cr-MOF/Gr

The XRD pattern of the Cr-MOF/Gr is mainly consistent with that Cr-MOF (Fig. 8). Also, No discernible diffraction peaks belonging to GO (normally at about 9.3°) has been detected in the pattern of Cr-MOF/Gr. The absence of GO characteristic peaks could be ascribed to the low GO content (10 wt%) and /or the exfoliation and reduction of GO in ethanol by sonication during the synthesis procedure as described before.

3.1.7 FTIR Spectra of the Prepared Cr-MOF Samples

FTIR spectra of the prepared Cr-MOF samples with the different Cr: BTC molar ratio (Fig. 9) show different characteristic bands, confirming the successful synthesis of MOF structure [6]:

1. Bands at 1610 cm^{-1}, and 1360 cm^{-1} are corresponding to C = O and C-O group of carboxylic acid after coordination of H_3BTC to the metal center.
2. The broad band at 3400 cm^{-1} assigned–OH groups, indicates the presence of water molecules, Furthermore, stretching vibration of –OH indicates the presence of hydrogen bonding after coordinated with Cr.
3. Bands at 590 and 729 cm^{-1} can be assigned to the Cr–O bonds of Cr-MOF compound, and 4) bands around 1700, and 1450 cm^{-1} Correspond to the (C = O) and (C-O) stretching frequency respectively for free carboxylic groups of H_3BTC [7].

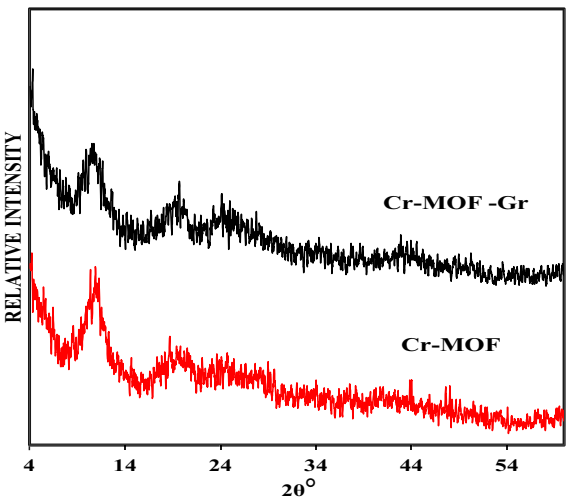

Fig. 8 XRD patterns of Cr-MOF& Cr-MOF/Gr samples

On the other hand, the decrease of Cr: BTC molar ratio from 2 to 1, lead to a slight decrease in the intensity of the bands. Also, the increase of Cr: BTC molar ratio from 2 to 3 lead to a slight decrease of all the vibrational bands that attributed to the inhibition of MOF structure formation which in agreement with XRD data.

FT-IR spectra of Cr-MOF & Cr-MOF/Gr wt. ratio (9:1) samples (Fig. 10). Represent that the spectrum of Cr-MOF/Gr hybrid nanocomposite is quite similar to the spectrum

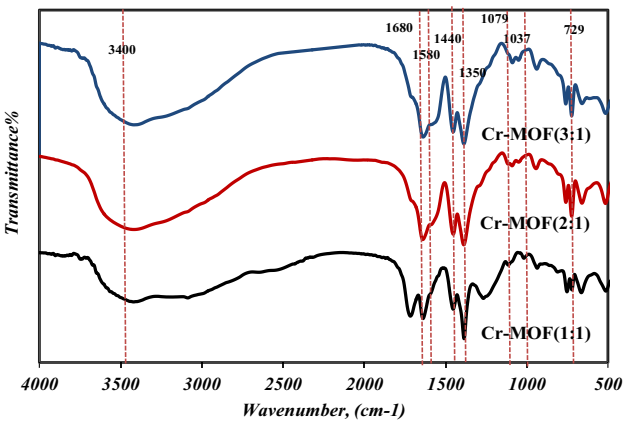

Fig. 9 FTIR spectra of the prepared Cr-MOF samples

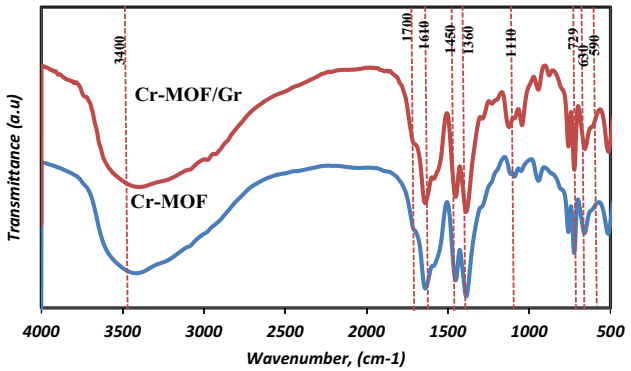

Fig. 10 FTIR spectra of Cr-MOF & Cr-MOF/Graphene samples

of the parent Cr-MOF (3400 cm^{-1}, 1700 cm^{-1}, 1610 cm^{-1}, 1450 cm^{-1},1360 cm^{-1}, 590 and 630 cm^{-1}) with other small intensity band related to the reduction of GO into Gr (3400 cm^{-1},1700 cm^{-1}). These data emphasize the successful synthesis of the Cr-MOF/Gr hybrid nanocomposites, as confirmed by XRD data.

The texture properties of the prepared Cr-MOF and Cr-MOF/Gr hybrid nano-composites were studied and the data are graphically illustrated in Fig. 11. The GO sample have no isotherm since it exhibits no porosity.

Both Cr-MOF and Cr-MOF/Gr hybrid nanocomposites show type-I isotherm, according to Brunauer's classification which characterize the predominant of micro pore structure without hysteresis loops. On the other hand, the prepared samples show a lower deviation of the v-t plot (Fig. 11) indicating a micro pore size distribution**.**

Also, the incorporation of GO in the prepared Cr-MOF samples lead to slightly decrease in surface area in parallel with the increase in pore. Moreover, BJH calculation shows unimodal pore size distribution with obvious porous distribution around 2 nm (Fig. 11).

Accordingly, the slightly decrease in surface area and increase of pore structure may be attributed to the incorporation of the low concentration of GO into MOF, in agreement wih Yujie Li data [9], as in the synthesis of nanocomposites, the epoxy groups of GO act as H_2O molecules, which usually coordinate with the central metal ions of the MOFs. During the linking procedure, delamination of the GO layers might occur, and the formed Gr layers didn't significantly disturb the crystallization/porosity of the MOF (Fig. 12).

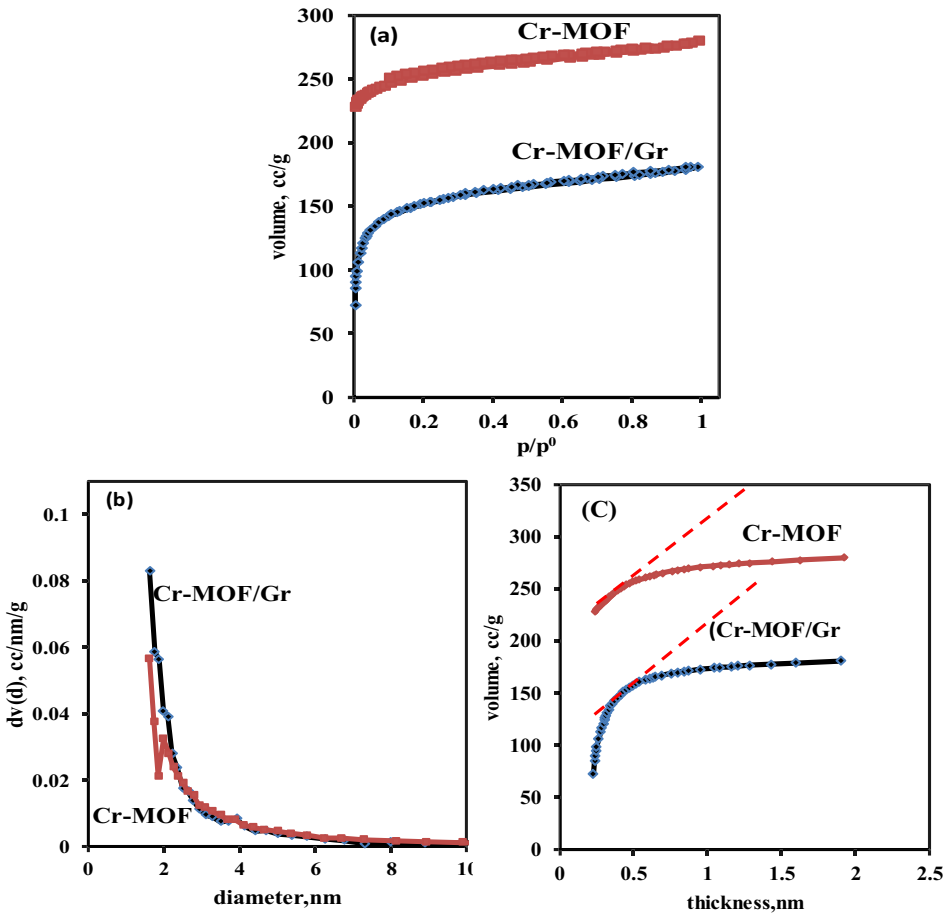

Fig. 11 **A** N_2 adsorption desorption isotherm, **B** PSD, and **C** v-t plot

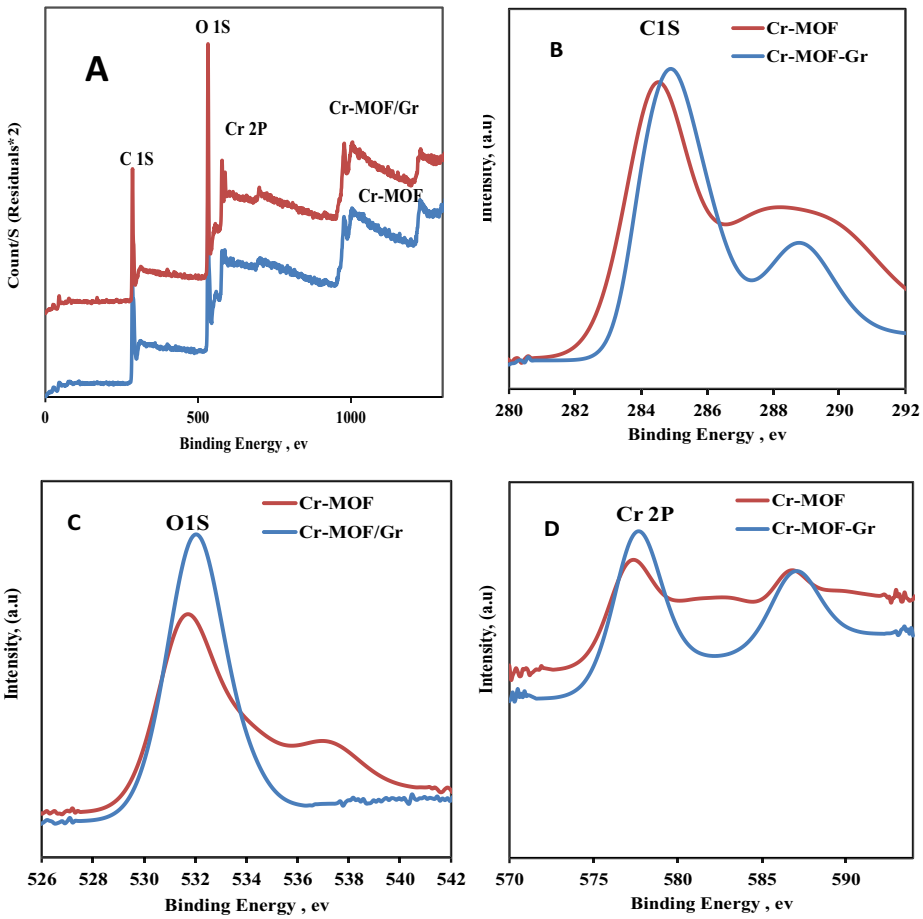

Fig. 12 **A** XPS survey analysis of Cr-MOF and Cr-MOF/Gr, **B** C1S spectra of Cr-MOF and Cr-MOF/Gr, **C** O 1 s spectra of Cr-MOF and Cr-MOF/Gr, **D** Cr 2p spectra of Cr-MOF and Cr-MOF/Gr

The X-ray photoelectron spectroscopy spectrum for Cr 2p For Cr-MOF represents two peaks at 587.02 eV and 576.63 eV (Fig. 37b). Meanwhile, for Cr-MOF/Gr, these two peaks are slightly shifted to 587.5 and 578.13 eV corresponded to typical binding energies for Cr^{3+}. Also, the slight shift in the binding energies points out an increment in the electron density around the Cr atom due the attractions between Cr^{3+} center and lone pair electrons of oxygen in the graphite oxide. No other oxidation states of chromium were observed, which means the stability of the chromium trimers during the functionalization of the linker and anchoring of graphite oxide.

3.2 Desulfurization Process

To compare the effectiveness of the prepared GO, MOF and MOF/Gr hybrid nanocomposite for adsorption of DBT from n-dodecane as model oil, DBT was chosen as a representative model of aromatic compounds containing-sulfur as it was the most common refractory compound in fuel after the HDS process it is found that the removal efficiency of the prepared GO is only 26 mgS/gm.

Figure 13 shows the effect of the Fe-MOF and Fe-MOF/Gr composite on the desulfurization process, the DBT adsorption experiment was conducted at room temperature for 300 min using an initial concentration of 1000 ppm (adsorbate) and the adsorbent weight was 20 g/L (optimum condition) from the previous published paper [12]. Actually, presence of graphene in the MOF composite has positive effect on sulfur removal. The removal efficiency increases from 62% to 95.6% using Fe-MOF and Fe-MOF/Gr (9:1) weight ratio.

The same effect was found when using Cr-MOF and Cr-MOF/Gr hybrid nanocomposite (Fig. 13). While, Cr-MOF/Gr shows best removal efficiency that reach 96.9% when using 20 g/L adsorbent, which confirm the vital effect of Gr in the performance of MOF/Gr as adsorbent for desulfurization process.

3.3 Diesel Fuel-Desulfurization process

As known, the commercial diesel fuel usually contains certain refractory sulfur compounds thiophene (TH),

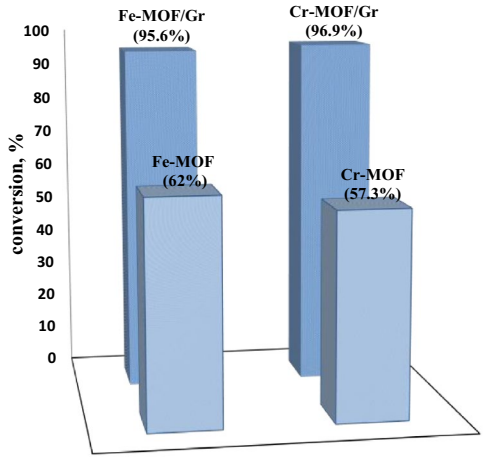

Fig. 13 Influence of the prepared samples on DBT adsorbtion (adsorbtion conditions: 25 °C, 300 min and 1000 ppm DBT)

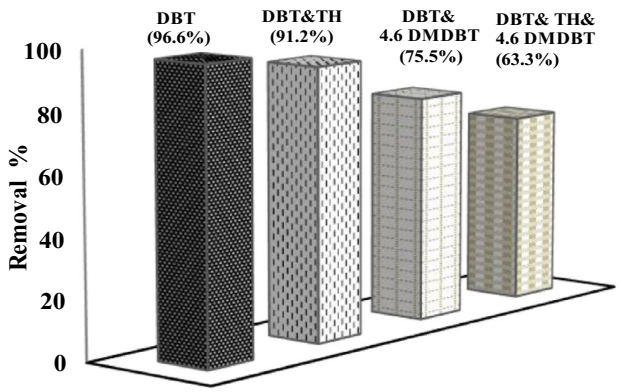

Fig. 14 Influence of the prepared MOF/Gr sample on the removal of TH, DBTand 4,6-DMDBT sulfur compounds

dibenzothiophene (DBT) and 4,6-dimethyldibenzothiophene (4,6-DMDBT), which causes environmental pollution [13].

From the previous result it can be concluded that, either the prepared Fe-MOF/Gr and/or Cr-MOF/Gr (9:1) weight ratio have relatively higher adsorption efficiency towards the removal of DBT than Cu-MOF/Gr [12], So the Cr-MOF/Gr adsorbent was selected to study the removal of more than sulfur compound that consist the model diesel oil.

The optimum adsorption conditions from our published paper [12] are chosen to carry out the desulfurization experimental processes of the model diesel oil either contain two and/or three organic sulfur compounds (DBT and TH), (DBT and 4,6-DMDBT), and (DBT, TH and 4,6-DMDBT).The adsorption experiments were conducted at room temperature for 300 min, an initial concentration of 1000 ppm model diesel oil (adsorbate) and on using 0.2 g of the selected Cr-MOF/Gr adsorbent one.

Data in Fig. 14, clarified that the removal of the aromatic sulfur compounds (thiophene (TH), dibenzothiophene (DBT) and 4.6 dimethyldibenzothiophene (4.6-DMDBT)) follows the order:

Dibenzothiophene > thiophene > 4.6 dimethyldibenzothiophene.

This behavior may be related to the double adsorption mechanism, i.e., physisorption and chemisorption. Taking thiophene for example, if sole weak physisorption is active, the adsorption capacity for thiophene should be higher than for dibenzothiophene due to the more steric restrictions of the dibenzothiophene molecule. However, when both physisorption and chemisorption occur in the adsorption process, and even chemisorption is dominant, the adsorption capacity for thiophene should be lower than for dibenzothiophene.In fact, the presence of additional aromatic ring in dibenzothiophene (as comparing with thiophene) increases the π-electron density, enhancing the probability of π-complexation to the exposed metal sites [14]. Moreover, the electron densities on the sulfur atoms of dibenzothiophene, and thiophene were 5.758, and 5.696 [15] respectively which probably enhances the direct interaction between the metal sites and the S-molecules. Despite of 4,6-dimethyldibenzothiophen have approximately less more electron density on sulfur atom (5.760) than dibenzothiophene the activity of dibenzothiophene is higher than 4,6-dimethyldibenzothiophene. This is may be due to the bonds between M and sulfur atoms was hindered by the alkyl groups that presented at 4 and 6 positions in 4,6-dimethyldibenzothiophene.

Accordingly, the desulfurization experiments for the diesel fuel fraction (from Cairo Oil Refining company, with boiling point (175–320 °C), and 600 ppm sulfur content) were carried out at reaction temperature range from 25 to 60ºC on using the selective active adsorbent Cr-MOF/Gr ranging from 0.2 to 2 gm.

10 ml of the feed (fuel diesel) with the required amount of the adsorbent was shacked for 300 min at the desired reaction temperature.

The total sulfur was determined using x-ray fluorescence sulfur meter (ASTMD-4294-98).

From the results (Fig. 15), it was found that, with the increase in the adsorbent amount from 0.2 to 1 gm the % removal of sulfur compound gradually increased, and followed by a marginal change with the increase in the adsorbent amount to 2 gm.

The increase in the adsorbent amount provides accessibility to large surface area, more adsorption sites, and active functional groups, thereby at the initial stage the adsorption uptakes gradually increases, followed by a marginal increment at the later stage. this is due to the

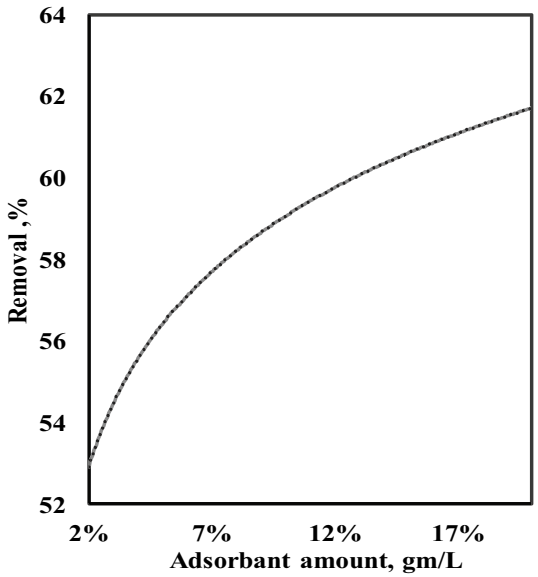

Fig. 15 Influence of adsorbent amount on the desulfurization of diesel feul (600 ppm sulfur)

attainment of equilibrium of sulfur concentration at the surface and bulk of the solution at the advanced stage.

In other words, this phenomenon is known as overcrowding of particles or solid concentration effect in the adsorption process**.** Accordingly, one-gram adsorbent amount is the most selected one for sulfur removal.

Figure 16 represents the effect of the reaction temperatures (range from 25 to 60 °C) on the desulfurization of the diesel oil at 300 min and the amount of adsorbent 1gm/10 ml. The data clarifies that, the removal % desulfurization at room temperature reaches 57.7%, whereas at 40 and 60 ºC decrease to 55 and 49% respectively. i.e.) the highest desulfurization is obtained at room temperature.

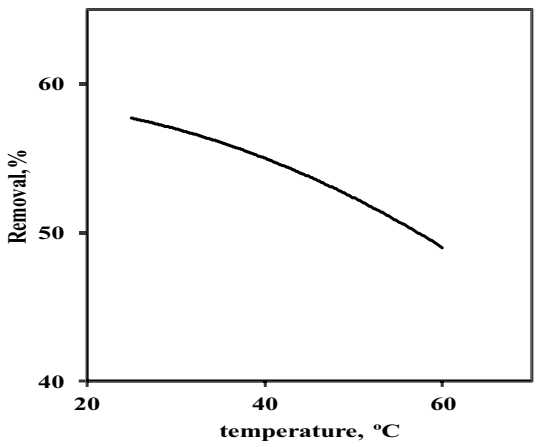

Fig. 16 Influence of Temperature on the desulfurization of diesel feul (600 ppm sulfur cpd)

Concurrently, the exothermic nature of the adsorption process is in parallel with the negative value of ΔH° (Table 2), verifying the more availability of adsorption at lower temperature. And the positive value of ΔS° suggests the randomness at the solid/liquid interface in the adsorption system. Also, the negative values of ΔG at reaction adsorption temperature 298, 313, and 333 K confirm the feasibility of the process and the spontaneous nature of adsorption. The increase of the negative value of ΔG° with the decrease in temperature established that the adsorption process becomes more favorable at lower temperature. Similar result is also reported by Waqas Ahmed, et al. [16]**,** they found that with the increase in the temperature from room temperature to 60 ºC the % desulfurization decreases from 63 to 58% on using Zn-Montmorollonite for adsorptive process.

From another point of view, Aromatics compounds in the diesel fuel have an effect on the combustion quality of the fuel and an increase in the amount of aromatics can have a negative impact on vehicle emissions. Moreover, fluorescent indicator adsorption method (FIA) was used to determine the three major type of hydrocarbons in the diesel fuel (before and after adsorption) which are saturates, olefins, and aromatics. Data represented that, the aromatic compounds were decreased from 6 to zero, olefins from 12 to 8.52 and saturates relatively increase from 82 to 91.48% after adsorption. The aniline point (AP) was also measured and the temperature increases from 75.5 (the mother diesel fuel) to 77.5 °C (the treated one). So, we can conclude that, using Cr-MOF/Gr for diesel desulfurization (optimum conditions: 300 min, 1gm of adsorbent, room temperature) not only decrease sulfur content but also decrease the aromatic content which lead to increase in the ignition quality, improves cold start performance and also reduce PM emission.

By applying the following Eqs. (3,4):

$$DI = AP\ (F^{\circ}) \times API/100 \tag{3}$$

$$CN = (DI \times 0.72) + 10 \tag{4}$$

where DI is the Diesel index, AP is the aniline point (Fº), API is American petroleum institute gravity, CN is the cetane number.

Taken into consideration, the aniline point and the aromatic content of the diesel fuel before and after treatment, it was found that the diesel index (DI) was increased from 66.8

Table 2 Adsorption thermodynamic of the desulfurized diesel fuel

T, Kelvin	ΔG	ΔH	ΔS
298	− 6470.64	− 5290.3	3.9
313	− 6514.18		
333	− 6607.21		

(the mother diesel fuel) to 68.3 (the treated one) and also the cetane number from 58.096 (the mother diesel fuel) to 59 (the treated one) which lead to an increase in the ignition quality, improves cold start performance and also reduce PM emission [17].

4 Conclusion

In this work, Fe-MOF & Cr-MOF and its graphene composites are prepared by using simple green solvothermal method and characterized by XRD, FT-IR, N_2 adsorption desorption isotherm and XPS. The characterization results indicate that the prepared MOF and MOF-Graphene adsorbent materials have the features of a metal–organic framework material. From the experimental results, both MOF, and both MOF-graphene show high adsorption abilities toward DBT at ambient temperatures. The Cr- MOF-Graphene adsorbent has achieved the highest adsorption removal of 96.6% at (300 min. room temperature, 20 g/l adsorbent), it was found that the adsorption removal for diesel fuel contain 600 ppm using Cr-MOF/Gr as an adsorbent at room temperature not only remove sulfur compounds but also decrease the aromatic content which has a positive effect on the diesel fuel characterization such as: aniline point from 75.5 (the mother diesel fuel) to 77.5 °C (the treated one), Diesel index from 66.8 (the mother diesel fuel) to 68.3 (the treated one) and also cetane number from 58.096 (the mother diesel fuel) to 59 (the treated one), which lead to increase in the ignition quality, improves cold start performance and also reduce PM emission.

Funding Open access funding provided by The Science, Technology & Innovation Funding Authority (STDF) in cooperation with The Egyptian Knowledge Bank (EKB).

References

1. I. Al Zubaidi, F.B. Tarsh, N. Darwish, B. Majeed, A. Sharafi, L. Chacra, J. Clean Energy Technol. (2013). https://doi.org/10.7763/JOCET.2013.V1.16
2. J.W. Yoon, Y.K. Seo, Y.K. Hwang, J.S. Chang, H. Leclerc, S. Wuttke, P. Bazin, A. Vimont, M. Daturi, E. Bloch, P.L. Llewellyn, C. Serre, P. Horcajada, J.M. Grenèche, A.E. Rodrigues, G. Férey, Angew. Chem. Int. Ed. (2010). https://doi.org/10.1002/anie.201001230
3. S.K. Shinde, D.-Y. Kim, M. Kumar, G. Murugadoss, S. Ramesh, A.M. Tamboli, H.M. Yadav, Polymers (2022). https://doi.org/10.3390/polym14030511
4. Z.C. Kampouraki, D.A. Giannakoudakis, V. Nair, A. Hosseini-Bandegharaei, J.C. Colmenares, E.A. Deliyanni, Molecules (2019). https://doi.org/10.3390/molecules24244525
5. A. Buchsteiner, A. Lerf, J. Pieper, J. Phys. Chem. B (2006). https://doi.org/10.1021/jp0641132
6. C. Petit, B. Mendoza, T.J. Bandosz, Chem. Phys. Chem. (2010). https://doi.org/10.1002/cphc.201000689
7. E. Rojas García, R. López Medina, M. May Lozano, I. Hernández Pérez, M.J. Valero, A.M. Maubert Franco, Materials (2014). https://doi.org/10.3390/ma7128037
8. R. Liu, X. Zhu, B. Chen, Sci. rep. (2017). https://doi.org/10.1038/srep40711
9. Y. Li, J. Miao, X. Sun, J. Xiao, Y. Li, H. Wang, Q. Xia, Z. Li, J. Phys. Chem. C. (2016). https://doi.org/10.1021/jp5045817
10. S.-H. Huo, X.-P. Yan, J. Mater. Chem. (2012). https://doi.org/10.1039/C2JM16513A
11. D. Wang, Y. Ke, D. Guo, H. Guo, J. Chen, W. Weng, Sens. Actuators B (2015). https://doi.org/10.1016/j.snb.2015.04.054
12. A.M. Matloob, D.R. Abdel-Hafiz, L. Saad, S. Mikhail, D. Guriguis, J. Hazard. Mater. (2019). https://doi.org/10.1016/j.jhazmat.2019.03.098
13. K.K. Sarda, A. Bhandari, K.K. Pant, S. Jain, Fuel (2012). https://doi.org/10.1016/j.fuel.2011.10.020
14. J. Xiao, C. Song, X. Ma, Z. Li, Ind. Eng. Chem. Res. (2012). https://doi.org/10.1021/ie202440t
15. F. Yu, R. Wang, Molecules (2013). https://doi.org/10.3390/molecules181113691
16. W. Ahmed, I. Ahmed, M. Ishaq, K. Ihsan, Arabian J. (2014). https://doi.org/10.1016/j.arabjc.2013.12.025
17. E.E. Ebrahiem, Y.A. Hakim, T.M. Aboul-Fotouh, M. Abd Elfattah, Egypt. J. Chem. (2022). https://doi.org/10.21608/EJCHEM.2021.87012.4206